


## Phase behavior of triblock copolymer and homopolymer blends: Effect of copolymer topology

Jiayu Xie<sup>\*</sup> and An-Chang Shi<sup>†</sup>*Department of Physics and Astronomy, McMaster University, Hamilton, Ontario, Canada L8S 4M1* (Received 20 August 2023; accepted 18 December 2023; published 11 January 2024)

Two distinct linear triblock copolymers with different block sequences, ABA or BAB, are obtained when two identical AB diblock copolymers are jointed at their B or A ends, respectively, resulting in three homologous, AB diblock, ABA, and BAB triblock copolymers with the same chemical composition but different topologies. We demonstrate that the topological effect on the phase behaviors of these copolymers is amplified when A homopolymers are added to the system. Specifically, the phase behaviors of binary blends composed of ABA or BAB linear triblock copolymers and A homopolymers are studied by using the random-phase approximation (RPA) and self-consistent field theory (SCFT). The RPA analysis predicts that the Lifshitz point for the ABA/A blends behaves like a second-order transition but that for the BAB/A blends behaves like a first-order transition. The Lifshitz point of the BAB/A mixtures is found to occur at a much lower homopolymer concentration than that of the ABA/A mixtures, indicating a poorer miscibility of the A homopolymers into the BAB than ABA triblocks, which is also confirmed by SCFT. For sphere-forming triblock copolymers mixed with homopolymers, the poorer miscibility and the more diffused distribution of the A homopolymers in the BAB/A blends result in a phase behavior drastically different from that of the ABA/A and AB/A blends. The ABA/A blends stabilize the Frank-Kasper (FK) phases similar to the AB/A blends, but the stability window of FK phases becomes negligibly small in the corresponding BAB/A blends. Our results demonstrate that the topological effect of block copolymers on the equilibrium phase behaviors can be more prominent in multi-component systems and thus more attention should be paid to copolymer topologies in the design of polymeric blends.

DOI: [10.1103/PhysRevMaterials.8.015601](https://doi.org/10.1103/PhysRevMaterials.8.015601)

## I. INTRODUCTION

Block copolymers composed of different blocks covalently bonded together are soft materials capable of self-assembling into ordered structures at the nanoscale [1,2]. The spontaneous ordering of block copolymers originates from the frustration due to opposing tendencies: chemically distinct blocks tend to phase separate, whereas the covalent bonds hold them together [3]. The equilibrium structure of block copolymers depends on various factors such as the volume fractions of the different blocks, the copolymer architecture, and temperature, etc. Such dependencies provide “knobs” by which the equilibrium morphology self-assembled from block copolymers can be regulated. Due to their rich phase behaviors, block copolymers not only hold promise in many applications such as lithography [4–7], photonics [8–10], and quantum materials [11,12], but also serve as an ideal platform to study the spontaneous ordering of matter.

The simplest block copolymer system is AB diblock copolymer melts. Due to extensive theoretical and experimental studies [13–20], it has been well-established that the equilibrium phase behavior of neat AB diblock copolymers is controlled by three parameters: (1) the A (or B) block composition  $f_A$  (or  $f_B$ ), (2) the interaction strength  $\chi N$  quantified by the product of the Flory-Huggins interaction parameter  $\chi$  and degree of polymerization  $N$ , and (3) the conformational asymmetry parameter  $\epsilon$ . Conformationally symmetric diblock copolymers ( $\epsilon = 1$ ) exhibit a phase-transition sequence from Dis  $\rightarrow$  HCP  $\rightarrow$  BCC  $\rightarrow$  HEX  $\rightarrow$  DG  $\rightarrow$  O<sup>70</sup>  $\rightarrow$  L as  $f_A$  changes from 0 to 0.5. Here Dis, HCP, BCC, HEX, DG, O<sup>70</sup>, and L represent disordered phase, hexagonal close-packed spheres, body-centered cubic spheres, hexagonal close-packed cylinders, double-gyroid networks, *Fddd* network, and lamellae [21]. For the case of  $\epsilon = 1$ , the  $f - \chi N$  phase diagram is symmetric about  $f = 0.5$ , and further increasing  $f$  from 0.5 to 1 traverses the same morphologies but with A and B inverted and the order reversed. Another well-studied system is the symmetric linear AB-type triblock copolymers, where each triblock chain is obtained by joining two identical diblock chains through either their A ends or B ends. With the same overall block composition, there are two distinct architectures, i.e., BAB and ABA, for an AB-type triblock copolymer. In contrast to the AB diblock copolymer melts, the  $f - \chi N$  phase diagram for the linear symmetric AB-type triblock copolymer melts becomes slightly asymmetric about  $f = 0.5$ , due to the topological nonequivalency

<sup>\*</sup>xiej33@mcmaster.ca<sup>†</sup>shi@mcmaster.ca

Published by the American Physical Society under the terms of the [Creative Commons Attribution 4.0 International](https://creativecommons.org/licenses/by/4.0/) license. Further distribution of this work must maintain attribution to the author(s) and the published article's title, journal citation, and DOI.

between the middle block and end blocks. However, the effect of this topological difference on the phase behavior is small and thus the phase diagram of the triblock copolymers remains largely analogous to that of the AB copolymers [21,22].

One effective route to expand accessible morphologies self-assembled from block copolymers is by mixing different polymers (copolymer/copolymer or copolymer/homopolymer) together. Extensive experimental and theoretical studies have demonstrated that block copolymer blends can stabilize new morphologies that are not stable in the system composed of the individual parent species alone [23–37]. The greatest advantage of the blending strategy for accessing new phases is that the architecture of each constituent polymeric species could remain simple, thus syntheses of complicated macromolecules could be avoided. The simplest polymeric blends that exhibit a rich phase behavior are binary AB diblock copolymer/A homopolymer blends. Depending on the block composition of the diblocks, the addition of appropriate homopolymers can stabilize a plethora of new morphologies including the Frank-Kasper (FK)  $\sigma$ , Laves C14 and C15, double diamond (DD), and plumber’s nightmare (P) phases [23,25,29,30,32,38–40].

Due to the incompatibility between the different components, an intrinsic feature of polymeric blends is their tendency to macrophase separate into two or more coexisting phases. Even for binary mixtures of two relatively simple polymeric components, the interplay between microphase and macrophase separations can lead to rather complex phase behaviors. For the simple binary AB/A blends, the addition of a small amount of homopolymers can induce order-order phase transitions, while the addition of an excessive amount of homopolymers generally results in the coexistence between a copolymer-rich ordered/disordered phase and a homopolymer-rich disordered phase [23,32,38]. One factor that strongly influences the solubility of the A homopolymers into the AB diblock copolymers as well as their spatial distribution is the ratio between the degrees of polymerization of the A homopolymer and the A block of the copolymer, i.e.,  $\xi = N_{A,\text{homo}}/N_{A,\text{diblock}}$ . For the case where  $\xi \ll 1$  (wet-brush regime), the A homopolymers penetrate into the A microdomains formed by the A blocks of the copolymers and the two components can remain miscible up to a high homopolymer concentration, while for the case where  $\xi \geq 1$  (dry-brush regime), the opposite is true [29,41–45]. Furthermore, the different behaviors of A homopolymers in the microdomains formed by the diblocks result in different equilibrium morphologies. For example, adding homopolymers in the dry-brush regime into BCC-forming AB copolymers could stabilize the FK  $\sigma$ , C14, and C15 phases; however, these complex spherical phases are replaced by the HEX phase if the added homopolymers are in the wet-brush regime [29,30,32].

Because the phase diagram of the symmetric AB-type triblock copolymers is similar to the phase diagram of neat AB diblock copolymers, it is reasonable to expect that the new morphologies accessed by adding homopolymers into AB copolymers could also be accessed by blending homopolymers and triblock copolymers. A natural question is how the topological difference between the ABA and BAB architectures affects the equilibrium morphology when the A homopolymers are added. Theoretical and experimental

studies of the AB-type triblock copolymer/A homopolymer mixtures have been carried out. However, most of the existing studies focused on the effect of adding homopolymers on the bridging fraction and mechanical properties of the triblock copolymers because of the commercial applications of triblock copolymers as thermoplastic elastomers [46,47]. On the other hand, compared to the AB diblock copolymers, less efforts have been made to investigate the morphological phase behavior of their homologous triblock copolymers mixed with homopolymers [48–50], and, to our knowledge, none has examined the role played by the topology or sequence distribution of the triblocks. Therefore, the effect induced by the topological difference between the ABA and BAB triblock copolymers on the phase behavior of their mixtures with A homopolymers remains unexplored.

In this paper, we examine the topological effect on the phase behavior of the binary blends composed of linear, ABA, or BAB symmetric triblock copolymers and A homopolymers. We employ the random-phase approximation (RPA) and the polymeric self-consistent field theory (SCFT), both applied to the freely jointed chain (FJC) model, to study the microphase and macrophase separations of three homologous systems, i.e., AB/A, ABA/A, and BAB/A blends. To focus on the effect of the copolymer topology, we consider the case where the copolymers in these three systems have the same overall block fractions. In addition, the degrees of polymerization of the two symmetric triblock chains are the same and both are twice that of the AB diblock chain. We first focus on the case where the copolymers are lamella-forming and construct phase diagrams on the  $\phi_2 - \chi_{AB}$  plane, where  $\phi_2$  is the homopolymer concentration, for the three systems to compare their phase behaviors. We then turn our attention to sphere-forming copolymers and examine the topological effect on the formation of the FK phases. In both cases, it is discovered that the AB/A and ABA/A blends have similar phase diagrams, whereas the BAB/A blends exhibit a drastically different phase behavior. Our results demonstrate that the topological effect in the neat AB-type triblock copolymers is amplified in their mixtures with A homopolymers and also provide insights into the topological effect in more complicated polymeric blends.

## II. THEORETICAL FRAMEWORK

In this section, we present the theoretical framework used in the current paper. We start with a description of the theoretical model based on the FJCs, followed by some details of the RPA calculation for the study of the stability line of the homogeneous phase and the SCFT calculation for the study of the relative stability of different phases. We will compare the phase behaviors of the three homologous ABA/A, BAB/A, and AB/A binary blends. Here the theoretical model is developed for the triblock copolymer/homopolymer blends. A similar theoretical formulation for the homologous AB/A blends can be found in our previous work [32].

### A. Theoretical model

We consider a binary blend composed of  $n_1$  linear symmetric triblock copolymers and  $n_2$  homopolymers in a volume

V. Each triblock copolymer is composed of  $N_A$  A segments and  $N_B$  B segments, resulting in a chain with  $N = N_A + N_B$  segments and  $N - 1$  bonds. Two distinct topologies or sequences of the triblock copolymer are considered here, with the A or B blocks as the bridging block (BAB or ABA), respectively. The overall volume fractions of the A and B blocks for a copolymer are given by  $f_A = f$  and  $f_B = 1 - f$ , respectively. Each homopolymer is composed of  $N_{Ah}$  A segments and the ratio between the number of A segments of an A homopolymer and that of a triblock copolymer is defined as  $\gamma = N_{Ah}/N_A = N_{Ah}/fN$ . We assume a uniform segment density  $\rho_0$  so  $\rho_0 V = n_1 N + n_2 \gamma f N$  due to the incompressibility condition. The average concentrations of the triblock copolymers and the A homopolymers are given by

$$\phi_1 = \frac{n_1 N}{\rho_0 V}, \quad \phi_2 = 1 - \phi_1 = \frac{n_2 \gamma f N}{\rho_0 V}.$$

The bonding potential between two adjacent segments in a polymer chain is given by

$$v_\alpha(R_i) = -k_B T \ln \delta(R_i - b_\alpha), \quad (1)$$

where  $R_i = |\mathbf{r}_{i+1} - \mathbf{r}_i|$  and  $b_\alpha$  is the Kuhn length of the segments of type  $\alpha$  with  $\alpha = A$  or B. The nonbonded interaction energy  $U$  takes the form

$$U = k_B T \rho_0 \chi_{AB} \int u(|\mathbf{r} - \mathbf{r}'|) \hat{\phi}_A(\mathbf{r}) \hat{\phi}_B(\mathbf{r}') d\mathbf{r} d\mathbf{r}', \quad (2)$$

where  $\hat{\phi}_\alpha(\mathbf{r}) = (1/\rho_0) \sum_i \delta(\mathbf{r} - \mathbf{r}_{\alpha i})$  is the density operator of  $\alpha$  segments,  $\chi_{AB}$  is the Flory-Huggins parameter quantifying the incompatibility between A and B segments and  $u(|\mathbf{r} - \mathbf{r}'|)$  describes the interaction potential as a function of intersegment distance. The conformational asymmetry parameter can be defined as  $\epsilon = b_A/b_B$ .

### B. Random-phase approximation

In general, the Helmholtz free-energy density functional of binary AB-type triblock copolymer/homopolymer blends can be written as an expansion with respect to small density fluctuations:

$$f = f^{(0)} + f^{(1)} + f^{(2)} + \dots \quad (3)$$

Of particular interest is the second-order term,

$$\begin{aligned} f^{(2)} &= \sum_{\alpha, \beta} \int \frac{d\mathbf{k}}{(2\pi)^3} \Gamma_{\alpha\beta}(\mathbf{k}) \delta\phi_\alpha(\mathbf{k}) \delta\phi_\beta(-\mathbf{k}) \\ &= \sum_{\alpha, \beta} \int \frac{d\mathbf{k}}{(2\pi)^3} S_{\alpha\beta}^{-1}(\mathbf{k}) \delta\phi_\alpha(\mathbf{k}) \delta\phi_\beta(-\mathbf{k}), \end{aligned} \quad (4)$$

where  $\Gamma_{\alpha\beta}(k)$ 's are the second-order coefficients,  $S_{\alpha\beta}(k)$ 's are the Fourier-transformed density-density correlation functions, and the subscript  $\alpha$  or  $\beta$  labels the blocks made up of the  $\alpha$  or  $\beta$  segments on different polymer chains. The RPA provides a systematic procedure to evaluate  $S_{\alpha\beta}^{-1}(k)$ 's, which can then be used to determine the stability line or spinodal of the system [51].

Following the formulation of Noolandi and coworkers [52,53], the resultant  $S_{\alpha\beta}^{-1}(\mathbf{k})$  computed by using RPA for binary AB-type copolymer/A homopolymer blends, denoted as  $S_{\text{RPA}}^{-1}(\mathbf{k})$ , is given by

$$S_{\text{RPA}}^{-1} = -u\chi - \frac{(g_{AA} + 2g_{AB} + g_{BB})\phi_1 + \gamma g_{AhAh}\phi_2}{2N\phi_1[(g_{AB}^2 - g_{AA}g_{BB})\phi_1 - \gamma g_{AhAh}g_{BB}\phi_2]}, \quad (5)$$

where the quantities  $g_{\alpha\beta}$ 's are related to the correlation functions of the ideal, noninteracting polymer chains, which will be introduced shortly. For the homogeneous phase,  $g_{\alpha\beta}$ 's only depend on the magnitude of  $\mathbf{k}$  and this  $k$  dependence has been made implicit in Eq. (5). The spinodal of the system is identified by the condition that the minimum of  $S_{\text{RPA}}^{-1}(k)$  equals zero. Denoting the  $k$  that minimizes  $S_{\text{RPA}}^{-1}(k)$  as  $k^*$ , this condition also corresponds to the threshold beyond which the homogeneous phase becomes unstable against the fluctuation characterized by  $k^*$ .

The general expression of  $g_{\alpha\beta}$  of a polymer chain is given by [51]

$$g_{\alpha\beta}(k) = \frac{1}{N_t^2} \sum_{i=1}^{N_t} \sum_{j=1}^{N_t} \Theta_i^\alpha \Theta_j^\beta P_{ij}, \quad (6)$$

where  $N_t$  is the total number of segments of the polymer chain and

$$\Theta_i^\alpha = \begin{cases} 1, & \text{if the } i\text{th segment is of type } \alpha, \\ 0, & \text{otherwise.} \end{cases} \quad (7)$$

In Eq. (6), the  $P_{ij}$  is the product of the  $k$ -space bond transition probabilities of all the segments that form the linear subchain bridging segments  $i$  and  $j$ . The current paper focuses on the case where all segments have the same Kuhn lengths, i.e., the bond transition probability  $p(k)$  is the same across the whole chain, so we simply have  $P_{ij} = p^{|i-j|}$ . For a FJC, the real-space bond transition probability and its Fourier-transformed version are given by

$$p(R) = \frac{1}{4\pi b^2} \delta(R - b), \quad (8)$$

$$p(k) = \frac{\sin(kb)}{kb}. \quad (9)$$

Using Eq. (6), the  $g_{\alpha\beta}$ 's for polymers with different architectures can be computed. For the A homopolymer, we have

$$g_{AhAh}(k) = \frac{2p(k)[p^{N_{Ah}}(k) - 1] - N_{Ah}p^2(k) + N_{Ah}}{N_{Ah}^2[p(k) - 1]^2}. \quad (10)$$

For an AB diblock copolymer, using the same segmental-number notations ( $N$ ,  $N_A$ , and  $N_B$ ) as the triblock for brevity,  $g_{AA}$  and  $g_{BB}$  have the same form as Eq. (10) but with Ah in the numerator replaced by A and B, respectively, and the  $N_{Ah}$  in the denominator replaced by  $N$ . The intersegment function  $g_{AB}$  is

$$g_{AB}(k) = \frac{p(k)[p^{N_A}(k) - 1][p^{N_B}(k) - 1]}{N^2[p(k) - 1]^2}. \quad (11)$$

For the symmetric ABA triblock copolymer,  $g_{BB}$  has the same form as that for the AB diblock, and the rest of the  $g_{\alpha\beta}$ 's are

given by

$$g_{AA}(k) = \frac{2p(k)[p^{\frac{N_A}{2}}(k) - 1][2 - p^{N_B}(k) + p^{\frac{N_A}{2} + N_B}(k)] - N_A p^2 + N_A}{N^2[p(k) - 1]^2}, \quad (12)$$

$$g_{AB}(k) = \frac{2p(k)[p^{\frac{N_A}{2}}(k) - 1][p^{N_B}(k) - 1]}{N^2[p(k) - 1]^2}. \quad (13)$$

Finally, for the symmetric BAB triblock copolymer, all the  $g_{\alpha\beta}$ 's have the same forms as those for the ABA triblock, but with A and B swapped.

### C. Self-consistent field theory

The SCFT is used to determine the phase boundaries between different phases. For systems undergoing both microphase and macrophase separations, it is convenient to work in the grand canonical ensemble where the thermodynamic control parameters are the chemical potentials of the triblock copolymers,  $\mu_1$ , and the A homopolymers,  $\mu_2$ . Within the scope of mean-field theory, the grand potential density of the system is expressed as [54]

$$\begin{aligned} \frac{N\Phi}{\rho_0 V k_B T} = & -e^{\mu_1/k_B T} Q_1 - e^{\mu_2/k_B T} Q_2 - \frac{1}{V} \int d\mathbf{r} [N\omega_A(\mathbf{r})\phi_A(\mathbf{r}) + N\omega_B(\mathbf{r})\phi_B(\mathbf{r}) \\ & - \chi_{AB} N \int u(|\mathbf{r} - \mathbf{r}'|)\phi_A(\mathbf{r})\phi_B(\mathbf{r}')d\mathbf{r}' + \eta(\mathbf{r})(1 - \phi_A(\mathbf{r}) - \phi_B(\mathbf{r}))], \end{aligned} \quad (14)$$

where  $Q_\kappa$  with  $\kappa = 1$  or  $2$  denotes the single-chain partition function of the triblock copolymer or the A homopolymer.  $\phi_\alpha(\mathbf{r})$  represents the ensemble average of the density operator  $\hat{\phi}_\alpha(\mathbf{r})$  and  $\omega_\alpha(\mathbf{r})$  is the auxiliary field conjugate to  $\phi_\alpha(\mathbf{r})$ .  $\eta(\mathbf{r})$  is the Lagrange multiplier enforcing the incompressibility condition. The total density profile of A segments in the system is given by

$$\phi_A(\mathbf{r}) = \phi_{At}(\mathbf{r}) + \phi_{Ah}(\mathbf{r}),$$

where  $\phi_{At}(\mathbf{r})$  and  $\phi_{Ah}(\mathbf{r})$  are the density profiles of the A segments from the triblock copolymers and the A homopolymers, respectively.

Minimizing the grand potential density with respect to the densities and auxiliary fields yields the following set of self-consistent equations:

$$\begin{aligned} N\omega_A(\mathbf{r}) &= \chi_{AB} N \int u(R)\phi_B(\mathbf{r} - \mathbf{R})d\mathbf{R} + \eta(\mathbf{r}), \\ N\omega_B(\mathbf{r}) &= \chi_{AB} N \int u(R)\phi_A(\mathbf{r} - \mathbf{R})d\mathbf{R} + \eta(\mathbf{r}), \\ \phi_A(\mathbf{r}) &= \frac{e^{\omega_A(\mathbf{r})}}{N} \sum_i^{N_A} q_1(i, \mathbf{r})q_1^\dagger(i, \mathbf{r}) \\ &+ e^{\mu/k_B T} \frac{e^{\omega_A(\mathbf{r})}}{N} \sum_{i=1}^{N_{Ah}} q_2(i, \mathbf{r})q_2^\dagger(i, \mathbf{r}), \\ \phi_B(\mathbf{r}) &= \frac{e^{\omega_B(\mathbf{r})}}{N} \sum_i^{N_B} q_1(i, \mathbf{r})q_1^\dagger(i, \mathbf{r}), \\ \phi_A(\mathbf{r}) + \phi_B(\mathbf{r}) &= 1, \end{aligned} \quad (15)$$

where  $\mathbf{R} = \mathbf{r} - \mathbf{r}'$  and  $R = |\mathbf{R}|$ . It is noted that the chemical potential  $\mu_1$  has been set to 0 by using the incompressibility condition so the subscript of  $\mu_2$  has been dropped for brevity. The concrete form for the summations over the segments of the triblock copolymer in Eqs. (15) depends on the architec-

ture of the chain. Specifically, for ABA copolymer, we have

$$\begin{aligned} \sum_i^{N_A} &= \sum_{i=1}^{N_A/2} + \sum_{i=N_A/2+N_B+1}^{N_A+N_B}, \\ \sum_i^{N_B} &= \sum_{i=N_A/2+1}^{N_A/2+N_B}, \end{aligned}$$

and for BAB copolymer, we have

$$\sum_i^{N_A} = \sum_{i=N_B/2+1}^{N_B/2+N_A},$$

$$\sum_i^{N_B} = \sum_{i=1}^{N_B/2} + \sum_{i=N_B/2+N_A+1}^{N_A+N_B}.$$

In Eqs. (15), the forward propagator  $q(i, \mathbf{r})$  is computed by iterating the equation

$$q_\kappa(i+1, \mathbf{r}_{i+1}) = e^{-\omega_\alpha(\mathbf{r}_{i+1})} \int d\mathbf{r}_i p_\alpha(\mathbf{r}_{i+1} - \mathbf{r}_i) q_\kappa(i, \mathbf{r}_i), \quad (16)$$

with the initial condition  $q_\kappa(1, \mathbf{r}) = \exp[-\omega_\alpha(\mathbf{r})]$ , where  $p_\alpha(\mathbf{r}_{i+1} - \mathbf{r}_i) (= p_\alpha(|\mathbf{r}_{i+1} - \mathbf{r}_i|) = p_\alpha(R))$  is the bond transition probability in Eq. (8). The backward propagator is computed similarly by performing the iterations in the opposite direction along the chain. With the propagators, the single-chain partition function  $Q_\kappa$  is calculated via

$$Q_\kappa = \frac{1}{V} \int d\mathbf{r}_{N_\kappa} q_\kappa(N_\kappa, \mathbf{r}_{N_\kappa}), \quad (17)$$

and the average concentrations of the different species are calculated by  $\phi_1 = Q_1$  and  $\phi_2 = 1 - \phi_1$ .

The interaction potential is chosen to have a Gaussian form

$$u(R) = \left( \frac{3}{2\pi r_0^2} \right)^{\frac{3}{2}} e^{-\frac{3R^2}{2r_0^2}}, \quad u(k) = e^{-\frac{k^2 r_0^2}{6}},$$



which is normalized in the real space, i.e.,  $\int u(R)d\mathbf{R} = 1$ . Throughout the current paper,  $r_0 = \sqrt{3}b_A$  is chosen and kept fixed.

The SCFT equations, i.e., Eqs. (15), are solved numerically by using the pseudospectral method combined with the variable-cell Anderson mixing for the FJCs. A detailed description of the numerical techniques can be found in our previous work [32]. For the construction of SCFT phase diagrams, various initial density fields corresponding to a set of candidate phases are used as inputs to Eqs. (15), which are then numerically solved to obtain the converged grand potential densities for these phases. A list of schematics for all the ordered candidate phases considered in this paper, along with the numbers of grid points used to discretize their unit cells in the SCFT calculations, is provided in Table S1 in the Supplemental Material [55]. Phase transition boundaries are determined by comparing the converged grand potential densities. Different sets of candidate phases are used for different scenarios, which will be introduced later.

For the purpose of the current paper, we restrict to the linear symmetric triblock copolymer with equal Kuhn lengths ( $b_A = b_B$ ), viz. the triblock is also conformationally symmetric ( $\epsilon = 1$ ). We also fix the total number of segments of the triblock chain to be 160. Under these restrictions, the free parameters of the binary AB-type triblock copolymer/A homopolymer mixtures include the A-block composition of the triblock ( $f$ ), the triblock topology (ABA or BAB), the total numbers of segments of the homopolymer ( $N_{Ah}$ ), the Flory-Huggins interaction parameter ( $\chi_{AB}$ ), and the homopolymer concentration ( $\phi_2$ ). Because the ABA and BAB triblocks considered here can be viewed as two identical diblocks covalently linked through their B and A ends, respectively, it is informative to also consider the homologous binary AB/A blends. To make a direct comparison, all the parameters of the diblock/homopolymer blends are chosen to be the same as those of the triblock/homopolymer blends except that the diblock chain is obtained by cutting the triblock chain in half. Therefore, each AB diblock has 80 segments and the same  $f$  as the triblocks (and thus  $N_{Ad} = N_A/2$ ). A convenient parameter to be defined is the segmental-number ratio  $\xi$  between the homopolymer and the A block of the AB diblock copolymer, i.e.,  $\xi = N_{Ah}/N_{Ad}$ . In the AB/A blends, the A homopolymers have the wet-brush behavior when  $\xi \ll 1$  and the dry-brush behavior when  $\xi \gtrsim 1$ .

### III. RESULTS AND DISCUSSION

We first consider the case with  $f = 0.45$  ( $N_A = 2N_{Ad} = 72$ ) so all the copolymers are lamella-forming. Figure 1 displays two phase diagrams in the  $\phi_2 - \chi_{AB}$  plane for two values of  $\xi$ , i.e.,  $\xi = 0.5$  ( $N_{Ah} = 18$ ) and  $\xi = 1$  ( $N_{Ah} = 36$ ), corresponding to the wet-brush and dry-brush regimes, respectively. Here the spinodal curve of a system signifies the point at which the homogeneous phase becomes unstable against fluctuations characterized by some wave vector  $k^*$ . For the binary mixtures considered in our paper, the spinodals can be classified into two types denoted by the solid and dashed lines in Fig. 1. The solid lines indicate the instability of the disordered phase against microphase separation, identified by  $S_{RPA}^{-1}(k)$  first becoming negative at a nonzero  $k^*$ . In contrast,

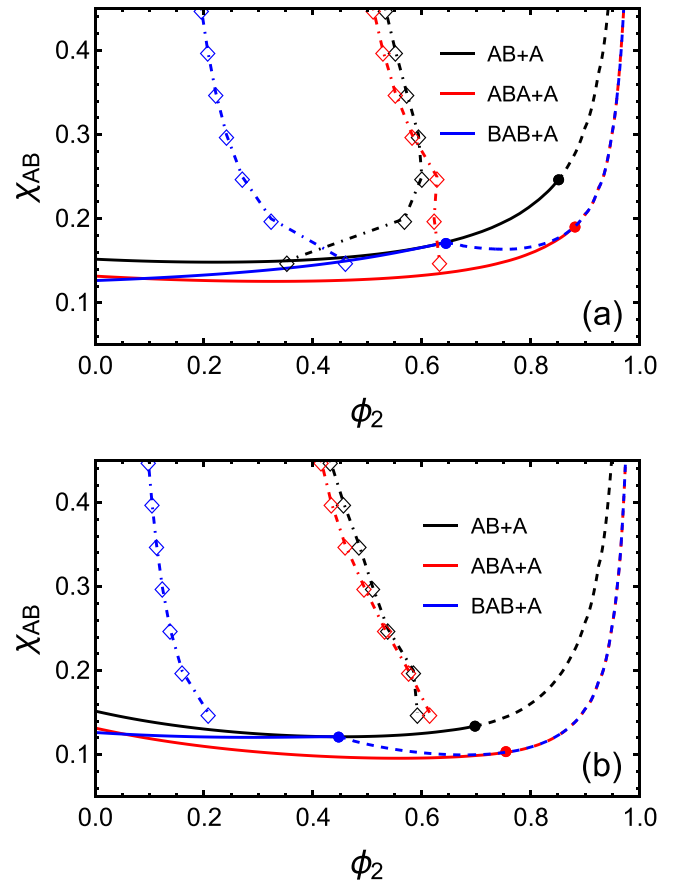


FIG. 1. The  $\phi_2 - \chi_{AB}$  phase diagrams with (a)  $\xi = 0.5$  ( $N_{Ah} = 18$ ) and (b)  $\xi = 1$  ( $N_{Ah} = 36$ ), corresponding to the wet-brush and dry-brush regimes, respectively. The RPA-evaluated spinodal of each system is composed of a portion on the left characterized by a nonzero  $k^*$  (solid line) and a portion on the right characterized by a zero  $k^*$  (dashed line). The two portions are joined at the Lifshitz point (solid circle). The dash-dotted lines are the L- $2\phi$  boundaries evaluated by SCFT for different systems.

the dashed lines indicate the instability of the disordered phase against macrophase separation corresponding to  $k^* = 0$ . The point on the spinodal curve separating these two behaviors is the Lifshitz point, marked by a solid circle in the phase diagrams. Besides the spinodals, the phase boundaries between the L phase and the two-phase coexistence ( $2\phi$ ) region are also evaluated by SCFT and presented in Fig. 1 as dash-dotted lines. We note that in constructing the diagrams in Fig. 1, we only considered the L phase as the candidate ordered phase competing with the Dis phase for simplicity. Although other morphologies such as the network phases and HEX phase might be stable at large  $\phi_2$ , we expect their stability windows to be small with the chosen parameters for most of the included  $\chi_{AB}$  values, and thus they will not drastically, if at all, shift the boundaries between the overall ordered phases and their  $2\phi$  region with the homopolymer-rich disordered phase. In determining the L- $2\phi$  boundaries in Fig. 1, we found that for the ABA/A and AB/A blends, it becomes very hard to converge the L phase at the region very close to the boundaries especially at higher  $\chi_{AB}$ . Whenever the L phase could not be converged beyond the L- $2\phi$  boundaries, we performed the

SCFT calculation for the L phase as close to the boundaries as we could and then used extrapolation to find the location of the boundaries approximately. For the BAB/A phase, this issue does not exist and the L phase can converge easily within certain range beyond the L-2 $\phi$  boundaries.

A common feature of the spinodal curves in Fig. 1 is that they are characterized by a nonzero  $k^*$  when  $\phi_2$  is small (solid lines), and, as  $\phi_2$  is increased,  $k^*$  drops to zero at the Lifshitz point (solid circles), after which  $k^*$  stays at zero upon further increasing  $\phi_2$  (dashed lines). This reflects the fact that there is a threshold of the amount of homopolymers the micro-domains formed by the copolymers can accommodate, beyond which the two components tend to phase separate macroscopically. A comparison between the two diagrams shows clearly a shift of the Lifshitz point to smaller  $\phi_2$  for all blends in Fig. 1(b) compared to Fig. 1(a). This expanded instability of the disordered phase against macrophase separation is consistent with the enhanced tendency to macrophase separate in the AB/A system when the A homopolymers become longer, both observed experimentally [29,42] and predicted theoretically [23,32]. Moreover, a comparison between different systems in the same diagram reveals that the Lifshitz points for the AB/A and ABA/A blends occur at similar  $\phi_2$ 's, which are noticeably higher than the  $\phi_2$  at which the Lifshitz point for the BAB/A blends occurs. For instance, in Fig. 1(a), corresponding to the wet-brush regime, the black and red circles are located at  $\phi_2 \sim 0.86$  while the blue one is at  $\phi_2 \sim 0.64$ , which differ by  $\Delta\phi_2 \sim 0.22$ . In Fig. 1(b), despite that all the Lifshitz points shift leftwards, the gap between their  $\phi_2$ 's still exists and slightly enlarges, i.e.,  $\Delta\phi_2 \gtrsim 0.25$ . This indicates that the BAB/A blends have a stronger tendency to macrophase separate than the AB/A and ABA/A blends.

The SCFT-predicted L - 2 $\phi$  boundaries for the three systems, denoted by the dash-dotted curves in Fig. 1, behave consistently with their RPA-predicted spinodals and Lifshitz points. As  $\xi$  changes from 0.5 [Fig. 1(a)] to 1 [Fig. 1(b)], all the L - 2 $\phi$  boundaries shift towards smaller  $\phi_2$ , clearly demonstrating a poorer miscibility of the copolymers and homopolymers. This behavior is consistent with the shift of the Lifshitz points. The diagrams also show that the L - 2 $\phi$  boundaries for the AB/A and ABA/A blends locate very near to each other for most of the  $\chi_{AB}$  range explored, except the region near  $\chi_{AB} \sim 0.15$  in Fig. 1(a), in which the L - 2 $\phi$  boundary for the AB/A starts to shift to the left of that for the ABA/A. This behavior at  $\chi_{AB} \sim 0.15$  may be a result of excluding the non-lamella phases in our calculations. More notably, the L - 2 $\phi$  boundary for the BAB/A blends appears at a significantly smaller  $\phi_2$  compared to those for the AB/A and ABA/A mixtures, regardless of  $\xi$ . This observation also coincides with the discovery that the homogeneous phase starts to become unstable against macrophase separation at a much lower  $\phi_2$  in the BAB/A blends compared to the other two systems. Combining the results from both the spinodals and L-2 $\phi$  boundaries, we conclude that for the binary AB/A blends linking the AB diblock chains through their B ends forming ABA triblocks roughly preserves the miscibility of the blends, whereas linking the diblocks through their A ends forming BAB triblocks drastically reduces the miscibility of the blends. Because the ABA and BAB triblocks have the same block composition and are both homologous to the AB

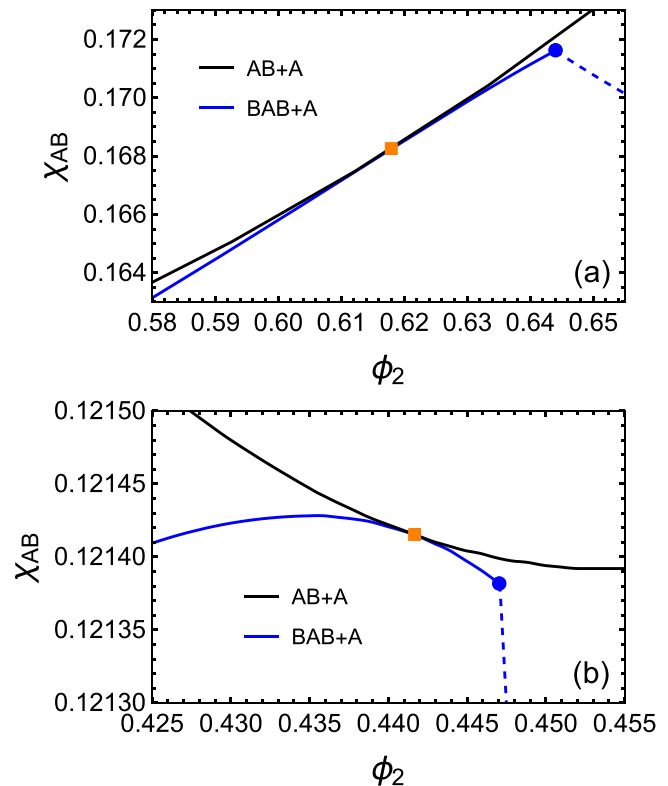


FIG. 2. The zoomed-in view of (a) Fig. 1(a) and (b) Fig. 1(b) in the vicinity of the Lifshitz point of the BAB/A system. The orange square in each diagram marks the estimated tangential point between the spinodals of the AB/A and BAB/A blends by interpolation.

diblock, the difference between their phase behaviors is entirely rooted in the topology or block sequence of the triblock copolymers.

An examination of the spinodal curves shown in Fig. 1 reveals another interesting behavior due to the topology of the copolymers. As  $\phi_2$  is increased from 0, the spinodal curve of the BAB/A blends gradually approaches that of the AB/A blends. These two curves intersect at roughly the same location of the Lifshitz point of the BAB/A system. At its Lifshitz point, the BAB/A spinodal curve exhibits an abrupt change in its slope, and it gradually approaches and eventually overlaps with the ABA/A spinodal curve upon further increasing  $\phi_2$ . For a clearer view, two zoomed-in plots showing the vicinity of the BAB/A Lifshitz points (blue solid circles) in Figs. 1(a) and 1(b) are provided in Figs. 2(a) and 2(b), respectively. Subject to numerical errors, our result suggests that the spinodals of the AB/A and BAB/A systems are tangential at their intersection, which is marked by a solid orange square in Fig. 2. The BAB/A Lifshitz point occurs very close to and after the tangential point between the BAB/A and AB/A spinodals, as seen in both Figs. 2(a) and 2(b).

To understand the discontinuous change in the slope of the BAB/A spinodal curve at the Lifshitz point, we take the  $\xi = 1$  case as an example and plot  $k^*$  as a function of  $\phi_2$  for the ABA/A and BAB/A blends in Fig. 3. It is very interesting that the behavior of  $k^*$  as a function of  $\phi_2$  is qualitatively different for the BAB/A and ABA/A blends. For the case of ABA/A blends [Fig. 3(a)], the  $k^*$  reduces to zero continuously as  $\phi_2$  is

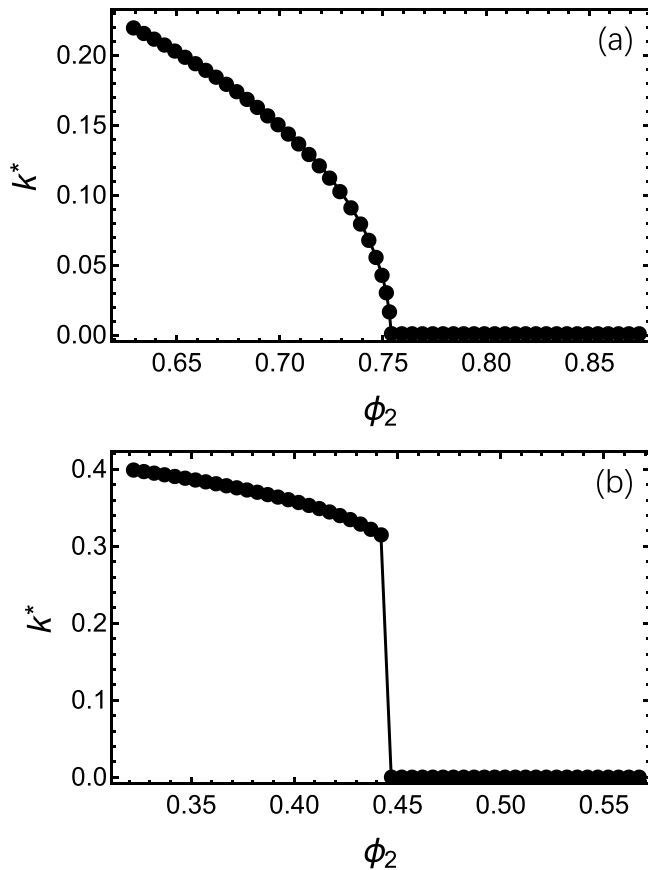


FIG. 3. Plots of  $k^*$  as a function of  $\phi_2$  for the (a) ABA/A and (b) BAB/A systems with  $\xi = 1$  ( $N_{Ah} = 36$ ). The Lifshitz point is defined as the position at which  $k^*$  turns from nonzero to zero. The behavior of  $k^*$  near the Lifshitz point of the AB/A blends has a similar feature to that of the ABA/A blends.

increased. This resembles the behavior of the order parameter of a system undergoing a second-order phase transition if  $k^*$  is regarded as the order parameter and  $\phi_2$  as the temperature. On the other hand, for the case of BAB/A blends as shown in Fig. 3(b), the  $k^*$  drops to zero discontinuously at the Lifshitz point, resembling a system undergoing a first-order phase transition. This difference stems from the behavior of the second-order correlation function  $S_{RPA}^{-1}(k)$  characterizing the fluctuations, which is shown in Fig. 4 for several representative values of  $\phi_2$  along the spinodals of the ABA/A and BAB/A systems with  $\xi = 1$ . In Fig. 4(a) for the ABA/A system,  $S_{RPA}^{-1}(k)$  only exhibits one minimum, which approaches zero continuously as  $\phi_2$  is increased from 0.735 to 0.77. For the BAB/A system,  $S_{RPA}^{-1}(k)$  exhibits one minimum when  $\phi_2$  is small, e.g.,  $\phi_2 = 0.395$ . However, a second local minimum, higher than the first one, appears at  $k = 0$  when  $\phi_2$  becomes larger, e.g.,  $\phi_2 = 0.437$ , as shown in Fig. 4(b). Further increasing  $\phi_2$  makes the second minimum become equal to the first one, at which the Lifshitz point is identified. When  $\phi_2$  is increased further, the minimum at  $k = 0$  becomes the global minimum (e.g.,  $\phi_2 = 0.452$  and 0.47) and the minimum at nonzero  $k$  eventually disappears (e.g.,  $\phi_2 = 0.47$ ). The switch of the global minimum of  $S_{RPA}^{-1}(k)$  from one to the other results in the sudden change in slope at the blue circles observed in

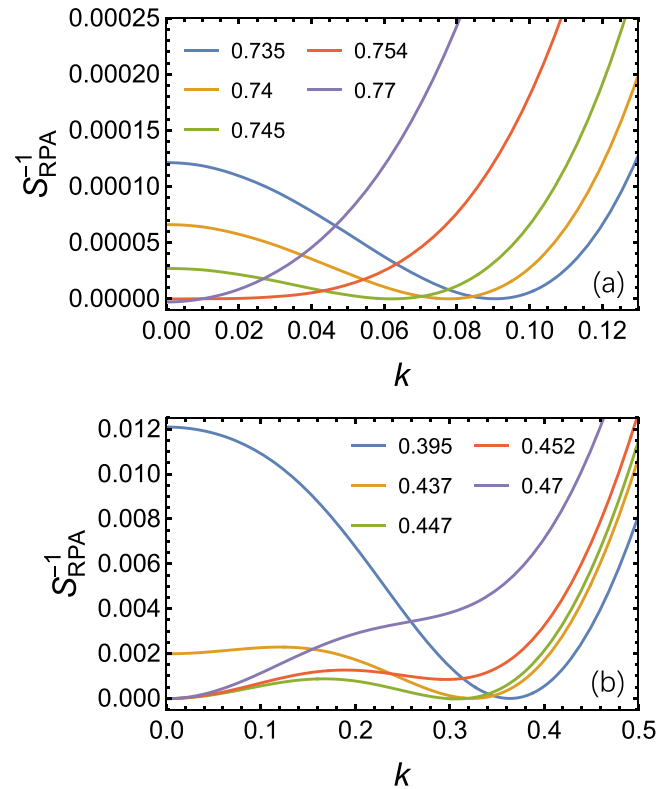


FIG. 4. Plots of  $S_{RPA}^{-1}(k)$  at several representative values of  $\phi_2$  along the spinodals of the (a) ABA/A and (b) BAB/A systems with  $\xi = 1$  ( $N_{Ah} = 36$ ).

Figs. 1 and 2. For the AB/A system, the Lifshitz point has the same second-order transition feature as that of the ABA/A system. Therefore, the spinodals of these two systems are smooth across the whole range of  $\phi_2$ .

The different natures of the Lifshitz points indicate different topographical characteristics of the free-energy landscapes of these blending systems, which, in turn, originate from the distinct chain topologies. In the case of the ABA/A and AB/A blends, the  $S_{RPA}^{-1}$  only has one minimum, that is, there is only one fluctuation mode leading the system from the homogeneous state to either microphase or macrophase separation. In contrast, for the BAB/A system, the mode driving the system to microphase separation coexists with the one driving it to macrophase separation within certain blend-composition range, e.g., from  $\phi_2 = 0.437$  to 0.452 in Fig. 4(b). When these two modes are comparable to each other, i.e., in the close vicinity of the Lifshitz point, the tendencies of the system to micro- and macrophase separate are in a close competition. In this regime, the BAB/A blends are expected to exhibit very interesting ordering dynamics, which would be of great interest for future research.

We now turn our attention to the case where the copolymers are sphere-forming by choosing  $f = 0.2$  ( $N_A = 2N_{Ad} = 32$ ) and focus on the effect of triblock topology on the equilibrium ordered morphology in the triblock copolymer/homopolymer blends. Previous studies have revealed the capability of binary AB/A blends to stabilize the FK phases when the added homopolymers are in the dry-brush regime [29,30,32]. Because we are interested in the topolog-

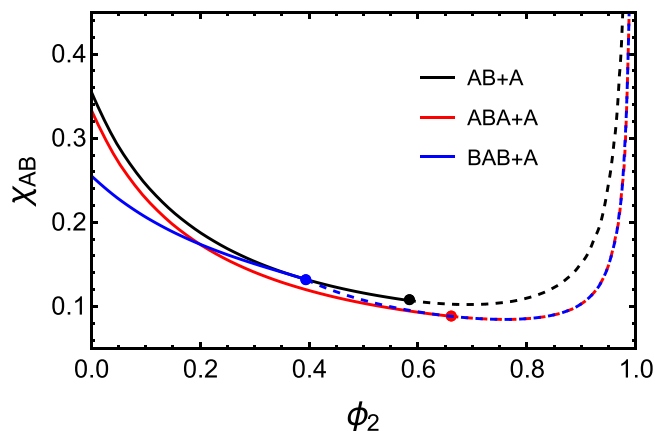


FIG. 5. Phase diagrams similar to those in Fig. 1 but for the sphere-forming systems, i.e.,  $f = 0.2$  ( $N_A = 2N_{Ad} = 32$ ), where the homopolymers are in the dry-brush regime, i.e.,  $\xi = 1$  ( $N_{Ah} = 16$ ). Only the RPA-predicted spinodals are included here and more detailed phase diagrams predicted by SCFT are in Fig. 6.

ical effect on the formation of the FK phases, we consider only the dry-brush case with  $\xi = 1$  ( $N_{Ah} = 16$ ). A preliminary examination of the phase behaviors of the three homologous systems, i.e., the AB/A, ABA/A, and BAB/A blends, is given by the spinodals obtained from the RPA (Fig. 5). Despite the overall change of their shapes, the three spinodals preserve the features revealed in the lamella-forming case. In particular, the relative locations of the Lifshitz points suggest that the BAB/A would still have a much poorer miscibility than the AB/A and ABA/A mixtures.

Figure 6 displays three detailed phase diagrams of the blends in the  $\phi_2 - \chi_{AB}$  plane obtained by using SCFT. These phase diagrams are constructed by considering a number of candidate phases including the Dis, HCP, BCC, and HEX as well as the FK  $\sigma$  and A15, and Laves C14 and C15 phases (Table S1). We note that the molecular parameters used in obtaining Fig. 6(a) are the same as those used for Fig. 3(a) in our previous paper [32]. The phase diagrams for the AB/A [Fig. 6(a)] and ABA/A [Fig. 6(b)] blends are remarkably similar. Despite a slight shift of the various phase boundaries towards lower  $\chi_{AB}$  and a slight expansion of the ordered region towards higher  $\phi_2$ , the overall phase behavior is preserved when the AB diblock copolymers in the AB/A blends are transformed into the ABA triblocks by linking each pair of diblocks through their B ends. Particularly, the ABA/A blends preserve the ability to stabilize the FK  $\sigma$ , C14, and C15 phases and the stability windows of these complex phases appear in the same order as in the AB/A blends when the homopolymer concentration is increased.

In strong contrast, the BAB/A blends have a drastically different phase behavior compared to both the AB/A and ABA/A blends [Fig. 6(c)]. Specifically, adding A homopolymers into the BAB triblocks induces a phase transition from the BCC to FK  $\sigma$  phase at  $\chi_{AB} \approx 0.225$  and  $\phi_2 \approx 0.07$ . The stability window of the  $\sigma$  phase is very small, spanning a narrow range of  $0.063 \lesssim \phi_2 \lesssim 0.085$  and  $0.209 \lesssim \chi_{AB} \lesssim 0.233$ . Furthermore, the HCP and Laves C14 and C15 phases are absent from the phase diagram. It is also observed that within the entire range of  $\chi_{AB}$  covered in Fig. 6(c), the ordered phase

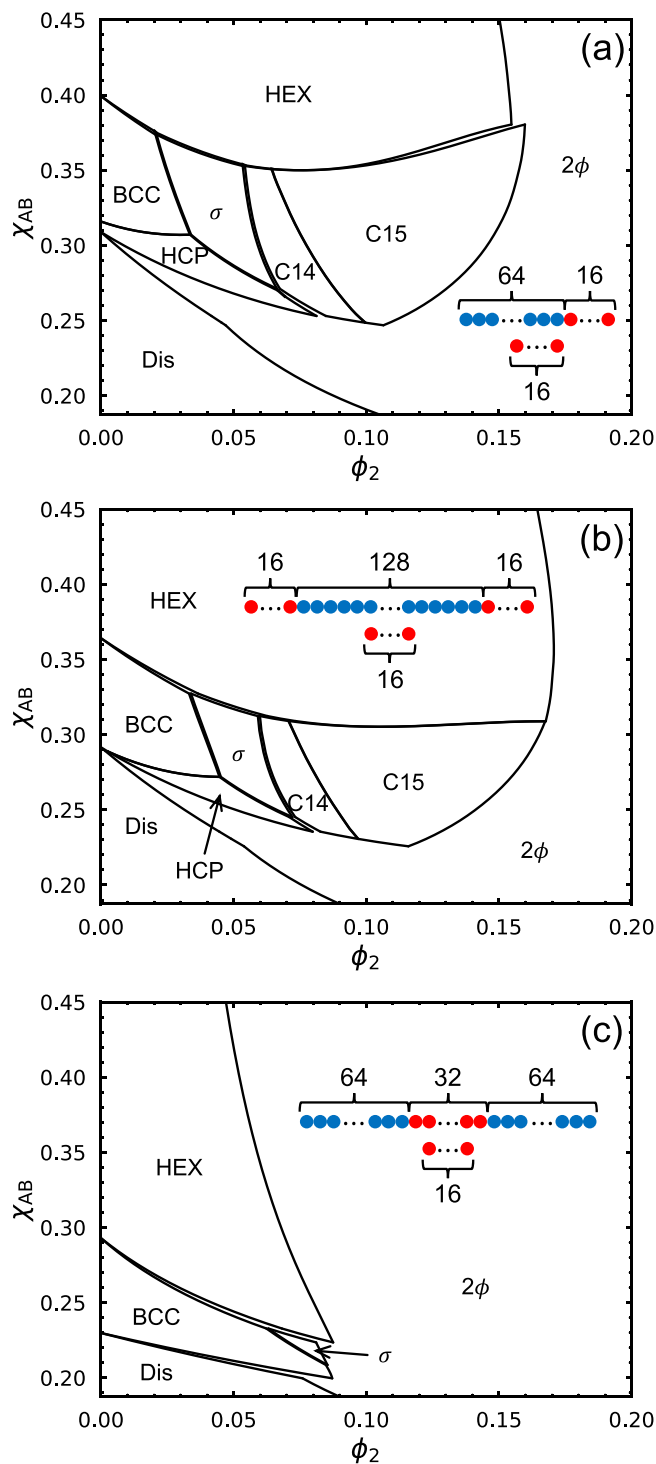


FIG. 6. Phase diagrams on the  $\phi_2 - \chi_{AB}$  plane showing the SCFT-predicted phase boundaries for the sphere-forming (a) AB/A, (b) ABA/A, and (c) BAB/A blends with the same parameters as those used for Fig. 5. Schematics of the polymer chains that each system are composed of are also included in its phase diagram. In the schematics, the A and B segments are denoted by red and blue beads, respectively, and the number of beads of each block is also shown.

region only expands to  $\phi_2 \approx 0.09$  upon the addition of the A homopolymers. Further increasing  $\phi_2$  induces macrophase separation. This more expanded  $2\phi$  region in the BAB/A



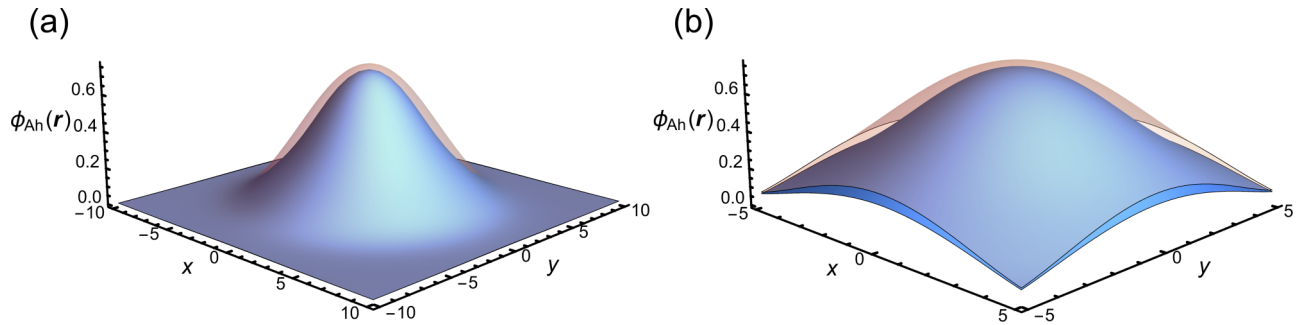


FIG. 7. Plots of the  $\phi_{Ah}(\mathbf{r})$ 's for the ABA/A (light red) and BAB/A (light blue) systems on the  $xy$  plane passing through the center of one representative spherical domain of the BCC phase. The density profiles are taken from the same point with  $\phi_2 = 0.07$  and  $\chi_{AB} = 0.297$  in Fig. 6(b) for the ABA/A blends and in Fig. 6(c) for the BAB/A blends. (b) is a zoomed-in view of the region near to the domain center in (a). In both (a) and (b),  $b_A$  is used as the unit of the  $x$  and  $y$  axes.

compared to the other two systems is consistent with the RPA prediction (Fig. 5). The depleted stability window of the FK phases, including the complete disappearance of the Laves C14 and C15 phases, is mainly due to the reduction of the single-phase region.

It is also observed from Fig. 6(c) that the BCC- $\sigma$  boundary shifts rightward to higher  $\phi_2$  and the order-disorder coexistence region at  $\phi_2 < 0.1$  diminishes compared to Fig. 6(b). Similar tendencies have been observed when the homopolymer molecular weight in the binary AB/A blends is decreased, which makes the homopolymers less concentrated in the A-rich domains [32]. Thus, we suspect that the homopolymers should also have a more diffused distribution in the BAB/A than in the ABA/A blends. To verify this conjecture, we compare the homopolymer distribution at the same point, i.e.,  $\phi_2 = 0.07$  and  $\chi_{AB} = 0.297$ , on the phase diagrams of these two systems, by plotting the  $\phi_{Ah}(\mathbf{r})$ 's of the ABA/A (light red) and BAB/A (light blue) systems on the  $xy$  plane passing through the center of one representative spherical domain of the BCC phase in Fig. 7. Specifically, Fig. 7(b) is a zoomed-in view of the region near to the domain center in Fig. 7(a) and  $b_A$  is used as the unit of the  $x$  and  $y$  axes. It is seen that the  $\phi_{Ah}(\mathbf{r})$  of the BAB/A blends is indeed lower than that of the ABA/A blends within a distance of more than  $5b_A$  away from the domain center, confirming a more diffused distribution of the A homopolymers in the BAB/A blends. This observed broader homopolymer distribution in the BAB/A system has a different origin from that induced by decreasing the molecular weight of the homopolymers, where the former should be related to the reduced configurational entropy of the A blocks of the triblock copolymers associated with the change of the molecular topology, while the latter is caused by the enhanced translational entropy of the homopolymers. The difference of these two mechanisms is also reflected by their different effects on the miscibility. Explicitly, decreasing  $N_{Ah}$  enhances the miscibility of the blends and thus expands the single-phase region towards higher  $\phi_2$ . On the contrary, the change of the triblock topology from ABA to BAB is observed to reduce the miscibility of the blends leading to a significantly smaller region of the single ordered phases.

To provide a quantitative measure of the homopolymer distribution, we compute the average homopolymer concen-

trations within the nonequivalent A-rich domains ( $\phi_2^D$ ) of the C15 phase as a function of  $\phi_2$  along the path of  $\chi_{AB} = 0.297$  and compare the results between the ABA/A and BAB/A systems in Fig. 8. For each system, the curves in Fig. 8 are evaluated before entering the  $2\phi$  region in the phase diagram. The FK phases are composed of more than one nonequivalent spherical domains with distinct sizes and shapes. Specifically, the C15 phase has two types of domains that differ significantly in volume. In Fig. 8, the large and small domains of the C15 phase are labeled by 1 and 2, respectively. It is observed that for both the ABA/A and BAB/A blends, the larger domains always have a higher average homopolymer concentration than the smaller ones, which has been similarly observed in the AB/A blends. Moreover, for both the small and large domains, the average homopolymer concentrations within the domains are constantly lower in the BAB/A than in the ABA/A system, which is consistent with the observation in Fig. 7.

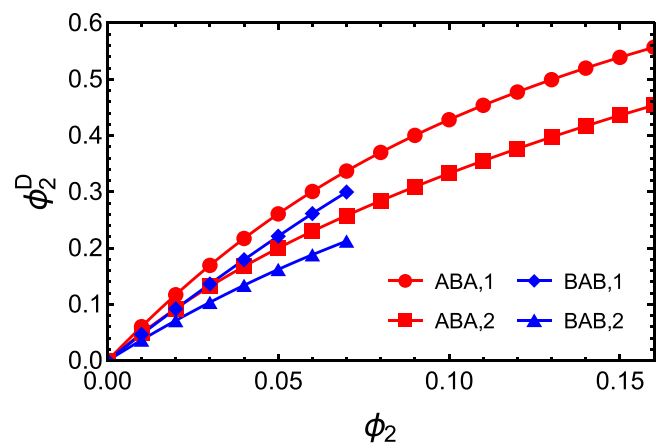


FIG. 8. The average concentrations of the homopolymers within the nonequivalent A-rich domains ( $\phi_2^D$ ) of the C15 phase as a function of  $\phi_2$  along the path of  $\chi_{AB} = 0.297$ . The curves for each system are evaluated before entering the  $2\phi$  region in the phase diagram. The large and small domains of the C15 phase are labeled by 1 and 2, respectively.

#### IV. CONCLUSION

In summary, we have studied the topological, or block sequence, effect on the phase behavior of binary blends composed of linear symmetric ABA or BAB triblock copolymers and A homopolymers by using the RPA and SCFT applied to the FJC model. Consistent phase behaviors have been obtained for lamella- and sphere-forming systems. For the case of lamella-forming systems, we examined the spinodals and  $L-2\phi$  boundaries of three polymeric mixtures, i.e., AB/A, ABA/A, and BAB/A, where the copolymers have the same block composition  $f$ . Our results indicate that the AB/A and ABA/A mixtures have similar miscibility and their Lifshitz points have a second-order transition feature; however, compared to AB/A and ABA/A, the BAB/A mixtures have noticeably poorer miscibility and a Lifshitz point with a first-order transition feature. This feature results in a discontinuous change in the slope of the BAB/A spinodal at its Lifshitz point. For the case of sphere-forming copolymers, we demonstrated that the topological effect has a large influence on the equilibrium morphology of the system. Particularly, the transition of the BCC to FK phases can be induced by adding A homopolymers into the ABA triblocks, which is similar to the phase behavior of the AB/A blends. In contrast, the FK phases are nearly absent in the BAB/A blends with the same block composition, which is due to a combined effect of the reduced miscibility and more diffused homopolymer distribution, both induced by the topological difference.

As demonstrated in previous SCFT studies [21,22], the phase behaviors of the homologous ABA and BAB triblock

copolymer melts are almost identical. The effect of triblock topology is reflected in small shifts of the phase boundaries, making the phase diagrams slightly asymmetric about  $f = 0.5$ . The results of the current paper suggest that the topological effect of triblock copolymers on the equilibrium phase behavior can be greatly amplified in their mixtures with A homopolymers. We believe that such amplification mechanism is generic, which is also expected to be valid in other multicomponent systems containing copolymers with more complicated architectures. The discoveries in the current paper provide a foundation for further research on the topological effect on the phase behaviors of more complex polymeric blends. Furthermore, recent advancements in polymer synthetic techniques have enabled copolymer samples with more precisely controlled block compositions and topologies [56–60]. The combination of theoretical and experimental studies will provide further understanding of the topological effect on the phase behaviors of polymeric blends containing block copolymers.

#### ACKNOWLEDGMENTS

This research was supported by the Natural Sciences and Engineering Research Council (NSERC) of Canada and was enabled in part by support provided by the facilities of SHARCNET [61]. A.C.S. thanks the Isaac Newton Institute for Mathematical Sciences, Cambridge, and the Aberystwyth University for support and hospitality during the programme GeomPack: Geometry and Packing in Material Structure and Biology, where work on this paper was undertaken. This work was supported in part by EPSRC Grant No EP/R014604/1.

- 
- [1] F. S. Bates and G. H. Fredrickson, Block copolymers—designer soft materials, *Phys. Today* **52**, 32 (1999).
  - [2] Y. Mai and A. Eisenberg, Self-assembly of block copolymers, *Chem. Soc. Rev.* **41**, 5969 (2012).
  - [3] A.-C. Shi, Frustration in block copolymer assemblies, *J. Phys.: Condens. Matter* **33**, 253001 (2021).
  - [4] J. Y. Cheng, C. Ross, E. Thomas, H. I. Smith, and G. J. Vancso, Fabrication of nanostructures with long-range order using block copolymer lithography, *Appl. Phys. Lett.* **81**, 3657 (2002).
  - [5] C. Tang, E. M. Lennon, G. H. Fredrickson, E. J. Kramer, and C. J. Hawker, Evolution of block copolymer lithography to highly ordered square arrays, *Science* **322**, 429 (2008).
  - [6] J. D. Cushen, I. Otsuka, C. M. Bates, S. Halila, S. Fort, C. Rochas, J. A. Easley, E. L. Rausch, A. Thio, R. Borsali *et al.*, Oligosaccharide/silicon-containing block copolymers with 5 nm features for lithographic applications, *ACS Nano* **6**, 3424 (2012).
  - [7] C. M. Bates, M. J. Maher, D. W. Janes, C. J. Ellison, and C. G. Willson, Block copolymer lithography, *Macromolecules* **47**, 2 (2014).
  - [8] A. Urbas, R. Sharp, Y. Fink, E. L. Thomas, M. Xenidou, and L. J. Fetters, Tunable block copolymer/homopolymer photonic crystals, *Adv. Mater.* **12**, 812 (2000).
  - [9] A. J. Parnell, A. Pryke, O. O. Mykhaylyk, J. R. Howse, A. M. Adawi, N. J. Terrill, and J. P. A. Fairclough, Continuously tuneable optical filters from self-assembled block copolymer blends, *Soft Matter* **7**, 3721 (2011).
  - [10] J. Lequieu, T. Quah, K. T. Delaney, and G. H. Fredrickson, Complete photonic band gaps with nonfrustrated ABC bottle-brush block polymers, *ACS Macro Lett.* **9**, 1074 (2020).
  - [11] R. P. Thedford, F. Yu, W. R. Tait, K. Shastri, F. Monticone, and U. Wiesner, The promise of soft-matter-enabled quantum materials, *Adv. Mater.* **35**, 2203908 (2023).
  - [12] F. Yu and U. Wiesner, The emerging field of block copolymer self-assembly-directed quantum materials, *Polymer* **281**, 126063 (2023).
  - [13] M. W. Matsen and M. Schick, Stable and unstable phases of a diblock copolymer melt, *Phys. Rev. Lett.* **72**, 2660 (1994).
  - [14] C. A. Tyler and D. C. Morse, Orthorhombic *Fddd* network in triblock and diblock copolymer melts, *Phys. Rev. Lett.* **94**, 208302 (2005).
  - [15] M. Takenaka, T. Wakada, S. Akasaka, S. Nishitsuji, K. Saijo, H. Shimizu, and H. Hasegawa, Orthorhombic *Fddd* network in diblock copolymer melts, [arXiv:cond-mat/0605268](https://arxiv.org/abs/cond-mat/0605268).
  - [16] S. Lee, M. J. Bluemle, and F. S. Bates, Discovery of a Frank-Kasper  $\sigma$  phase in sphere-forming block copolymer melts, *Science* **330**, 349 (2010).
  - [17] N. Xie, W. Li, F. Qiu, and A.-C. Shi,  $\sigma$  phase formed in conformationally asymmetric AB-type block copolymers, *ACS Macro Lett.* **3**, 906 (2014).
  - [18] S. Lee, C. Leighton, and F. S. Bates, Sphericity and symmetry breaking in the formation of Frank-Kasper phases from one component materials, *Proc. Natl. Acad. Sci.* **111**, 17723 (2014).

- [19] M. W. Schulze, R. M. Lewis III, J. H. Lettow, R. J. Hickey, T. M. Gillard, M. A. Hillmyer, and F. S. Bates, Conformational asymmetry and quasicrystal approximants in linear diblock copolymers, *Phys. Rev. Lett.* **118**, 207801 (2017).
- [20] M. W. Bates, J. Lequeieu, S. M. Barbon, R. M. Lewis, K. T. Delaney, A. Anastasaki, C. J. Hawker, G. H. Fredrickson, and C. M. Bates, Stability of the A15 phase in diblock copolymer melts, *Proc. Natl. Acad. Sci.* **116**, 13194 (2019).
- [21] M. W. Matsen, Effect of architecture on the phase behavior of AB-type block copolymer melts, *Macromolecules* **45**, 2161 (2012).
- [22] M. W. Matsen and R. Thompson, Equilibrium behavior of symmetric ABA triblock copolymer melts, *J. Chem. Phys.* **111**, 7139 (1999).
- [23] M. W. Matsen, Phase behavior of block copolymer/homopolymer blends, *Macromolecules* **28**, 5765 (1995).
- [24] D. Yamaguchi, S. Shiratake, and T. Hashimoto, Ordered structure in blends of block copolymers. 5. Blends of lamella-forming block copolymers showing both microphase separation involving unique morphological transitions and macrophase separation, *Macromolecules* **33**, 8258 (2000).
- [25] F. J. Martinez-Veracoechea and F. A. Escobedo, The plumber's nightmare phase in diblock copolymer/homopolymer blends. a self-consistent field theory study, *Macromolecules* **42**, 9058 (2009).
- [26] Z. Wu, B. Li, Q. Jin, D. Ding, and A.-C. Shi, Phase behavior of binary blends of diblock copolymers, *J. Phys. Chem. B* **114**, 15789 (2010).
- [27] Z. Wu, B. Li, Q. Jin, D. Ding, and A.-C. Shi, Microphase and macrophase separations in binary blends of diblock copolymers, *Macromolecules* **44**, 1680 (2011).
- [28] H. Takagi, K. Yamamoto, and S. Okamoto, Ordered-bicontinuous-double-diamond structure in block copolymer/homopolymer blends, *Europhys. Lett.* **110**, 48003 (2015).
- [29] A. J. Mueller, A. P. Lindsay, A. Jayaraman, T. P. Lodge, M. K. Mahanthappa, and F. S. Bates, Emergence of a C15 Laves phase in diblock polymer/homopolymer blends, *ACS Macro Lett.* **9**, 576 (2020).
- [30] G. K. Cheong, F. S. Bates, and K. D. Dorfman, Symmetry breaking in particle-forming diblock polymer/homopolymer blends, *Proc. Natl. Acad. Sci.* **117**, 16764 (2020).
- [31] A. P. Lindsay, R. M. Lewis III, B. Lee, A. J. Peterson, T. P. Lodge, and F. S. Bates, A15,  $\sigma$ , and a quasicrystal: Access to complex particle packings via bidisperse diblock copolymer blends, *ACS Macro Lett.* **9**, 197 (2020).
- [32] J. Xie and A.-C. Shi, Formation of complex spherical packing phases in diblock copolymer/homopolymer blends, *Giant* **5**, 100043 (2021).
- [33] J. Xie, Y. Li, and A.-C. Shi, Binary blends of diblock copolymers: An efficient route to complex spherical packing phases, *Macromol. Theory Simul.* **30**, 2100053 (2021).
- [34] C. T. Lai and A.-C. Shi, Binary blends of diblock copolymers: An effective route to novel bicontinuous phases, *Macromol. Theory Simul.* **30**, 2100019 (2021).
- [35] A. P. Lindsay, G. K. Cheong, A. J. Peterson, S. Weigand, K. D. Dorfman, T. P. Lodge, and F. S. Bates, Complex phase behavior in particle-forming AB/ABd'iblock copolymer blends with variable core block lengths, *Macromolecules* **54**, 7088 (2021).
- [36] J. Xie and A.-C. Shi, Phase behavior of binary blends of diblock copolymers: Progress and opportunities, *Langmuir* **39**, 11491 (2023).
- [37] J. Xie and A.-C. Shi, Theory of complex spherical packing phases in diblock copolymer/homopolymer blends, *Macromolecules* **56**, 10296 (2023).
- [38] M. W. Matsen, Stabilizing new morphologies by blending homopolymer with block copolymer, *Phys. Rev. Lett.* **74**, 4225 (1995).
- [39] F. J. Martinez-Veracoechea and F. A. Escobedo, Bicontinuous phases in diblock copolymer/homopolymer blends: Simulation and self-consistent field theory, *Macromolecules* **42**, 1775 (2009).
- [40] H. Takagi and K. Yamamoto, Effect of block copolymer composition and homopolymer molecular weight on ordered bicontinuous double-diamond structures in binary blends of polystyrene-polyisoprene block copolymer and polyisoprene homopolymer, *Macromolecules* **54**, 5136 (2021).
- [41] C. Berney, P. L. Cheng, and R. Cohen, Distribution of matrix homopolymer in block copolymers of spherical morphology, *Macromolecules* **21**, 2235 (1988).
- [42] T. Hashimoto, H. Tanaka, and H. Hasegawa, Ordered structure in mixtures of a block copolymer and homopolymers. 2. Effects of molecular weights of homopolymers, *Macromolecules* **23**, 4378 (1990).
- [43] H. Tanaka, H. Hasegawa, and T. Hashimoto, Ordered structure in mixtures of a block copolymer and homopolymers. 1. Solubilization of low molecular weight homopolymers, *Macromolecules* **24**, 240 (1991).
- [44] K. I. Winey, E. L. Thomas, and L. J. Fetters, Swelling of lamellar diblock copolymer by homopolymer: Influences of homopolymer concentration and molecular weight, *Macromolecules* **24**, 6182 (1991).
- [45] S. Koizumi, H. Hasegawa, and T. Hashimoto, Spatial distribution of homopolymers in block copolymer microdomains as observed by a combined SANS and SAXS method, *Macromolecules* **27**, 7893 (1994).
- [46] L. Kane, D. A. Norman, S. A. White, M. W. Matsen, M. M. Satkowski, S. D. Smith, and R. J. Spontak, Molecular, nanostructural and mechanical characteristics of lamellar triblock copolymer blends: effects of molecular weight and constraint, *Macromol. Rapid Commun.* **22**, 281 (2001).
- [47] J. Baetzold, I. Gancarz, X. Quan, and J. Koberstein, Mechanical property modification and morphology of poly(styrene-b-hydrogenated butadiene-b-styrene)/poly(hydrogenated butadiene) blends, *Macromolecules* **27**, 5329 (1994).
- [48] X. Quan, I. Gancarz, J. Koberstein, and G. Wignall, Effect of homopolymer molecular weight on the morphology of block copolymer/homopolymer blends, *Macromolecules* **20**, 1431 (1987).
- [49] S.-H. Lee, J. Koberstein, X. Quan, I. Gancarz, G. Wignall, and F. Wilson, Spatial distribution of a midblock-associating homopolymer blended into a triblock copolymer, *Macromolecules* **27**, 3199 (1994).
- [50] D. Norman, L. Kane, S. White, S. Smith, and R. Spontak, Triblock copolymer/homopolymer blends: Conformational changes, microstructural transition and macrophase separation, *J. Mater. Sci. Lett.* **17**, 545 (1998).
- [51] L. Leibler, Theory of microphase separation in block copolymers, *Macromolecules* **13**, 1602 (1980).

- [52] K. M. Hong and J. Noolandi, Theory of phase equilibria in systems containing block copolymers, *Macromolecules* **16**, 1083 (1983).
- [53] M. D. Whitmore and J. Noolandi, Theory of phase equilibria in block copolymer-homopolymer blends, *Macromolecules* **18**, 2486 (1985).
- [54] A.-C. Shi, Self-consistent field theory of inhomogeneous polymeric systems, *Variational Methods in Molecular Modeling*, edited by J. Wu (Springer, Singapore, 2017), p. 155.
- [55] See Supplemental Material at <http://link.aps.org/supplemental/10.1103/PhysRevMaterials.8.015601> for a list of schematics of the candidate phases considered, along with the numbers of grid points used to discretize their unit cells, in the SCFT calculations.
- [56] Y. Sun, R. Tan, Z. Ma, Z. Gan, G. Li, D. Zhou, Y. Shao, W.-B. Zhang, R. Zhang, and X.-H. Dong, Discrete block copolymers with diverse architectures: Resolving complex spherical phases with one monomer resolution, *ACS Cent. Sci.* **6**, 1386 (2020).
- [57] S. Duan, X. Yang, Z. Yang, Y. Liu, Q. Shi, Z. Yang, H. Wu, Y. Han, Y. Wang, H. Shen *et al.*, A versatile synthetic platform for discrete oligo- and polyesters based on optimized protective groups via iterative exponential growth, *Macromolecules* **54**, 10830 (2021).
- [58] D. Cai, J. Li, Z. Ma, Z. Gan, Y. Shao, Q. Xing, R. Tan, and X.-H. Dong, Effect of molecular architecture and symmetry on self-assembly: A quantitative revisit using discrete ABA triblock copolymers, *ACS Macro Lett.* **11**, 555 (2022).
- [59] Z. Ma, R. Tan, Z. Gan, D. Zhou, Y. Yang, W. Zhang, and X.-H. Dong, Modulation of the complex spherical packings through rationally doping a discrete homopolymer into a discrete block copolymer: A quantitative study, *Macromolecules* **55**, 4331 (2022).
- [60] D. Zhou, M. Xu, Z. Ma, Z. Gan, J. Zheng, R. Tan, and X.-H. Dong, Discrete Diblock Copolymers with Tailored Conformational Asymmetry: A Precise Model Platform to Explore Complex Spherical Phases, *Macromolecules* **55**, 7013 (2022).
- [61] <https://www.sharcnet.ca>.